Proceedings of the
Annual Stability Conference
Structural Stability Research Council
St. Louis, Missouri, April 16-20, 2013

Analytical Assessment of the Strength of Steel Truss Bridge Gusset Plates

Y.D. Kim[1], Y. Mentes[2], D.W. White[3], R.T. Leon[4]

Abstract

This paper investigates the strength of steel truss bridge gusset plates using finite element parametric test simulations validated against full-scale experimental tests. Numerous study cases are designed by varying the locations in the bridge and thus the corresponding loading scenarios, joint geometries including gusset thicknesses, member end details, member inclination angles, member connection lengths, free edge lengths, fastener strengths, corrosion patterns, and retrofit scenarios. The strengths obtained from the parametric studies are summarized and a number of recommendations are provided to improve current gusset plate design and rating procedures.

1. Introduction

The collapse of the I-35W Bridge in Minneapolis in August 2007 focused attention on the reliability and safety of truss bridges in the U.S. The failure investigations indicated that the collapse was initiated by buckling of the gusset plates at the U10 joint. These plates had inadequate thickness resulting from an error in the original design (Holt and Hartmann, 2008; NTSB, 2008). In the aftermath of the I-35W Bridge failure, the Federal Highway Administration (FHWA) issued a technical advisory emphasizing the need to check gusset plates in the load rating process of non-load path redundant trusses (FHWA, 2008). Subsequently, the National Transportation Safety Board issued a number of recommendations based on its comprehensive investigation (NTSB, 2008), and the FHWA issued guidance on gusset plate design and rating (referred to herein as the FHWA Guide) based on the best available information (FHWA, 2009). While it was generally acknowledged by experts that the FHWA Guide represented the best available knowledge on gusset plate design, it was also acknowledged that it may be overly conservative for some limit state checks. Therefore, to develop and improve design and rating procedures for gusset plate connections in steel truss bridges, a research project was launched which included laboratory as well as analytical studies of gusset plate joints. This research was performed under direction of the FHWA in collaboration with the National Cooperative Highway Research Program (NCHRP) Project 12-84 "Guidelines for the Load and Resistance Factor Design and Rating of Riveted and Bolted Gusset Plate Connections for Steel Bridges." This paper discusses the analytical research conducted at Georgia Institute of Technology in

[1] Assistant Professor, Georgia Perimeter College, <yoonduk.kim@gpc.edu>
[2] Senior Staff Engineer, MMI Engineering, <ymentes@mmiengineering.com>
[3] Professor, Georgia Institute of Technology <don.white@ce.gatech.edu>
[4] David H. Burrows Professor of Construction Engineering, Virginia Polytechnic Institute and State University <rleon@vt.edu>

support of NCHRP 12-84 and the synthesis of results from these studies. The specific focus of this effort was to evaluate the limit states response of steel truss bridge gusset plates over a wide range of potential configurations encountered in practice. This paper focuses on the compression resistance of gusset plates and the characterization of this resistance by simplified design equations.

2. Parametric Study Design

2.1 Joint Configurations

Three main truss types were selected for the parametric studies conducted in this research:

1) Warren with vertical members,
2) Pratt, and
3) Warren without vertical members.

Examination of available bridge plans indicated that longer continuous-span bridges generally have Warren configurations with or without vertical members (Mentes 2011). In addition, the NCHRP 12-84 project panel indicated that Warren trusses without verticals are more common in more recent construction, and that Pratt trusses are used mostly for shorter simple-span bridges. All of the cases considered in this research were double-gusset joint geometries representative of steel highway bridge trusses. Single-gusset geometries were not addressed directly in this work.

Given the above general truss configurations, representative joints were extracted from the following locations within hypothetical bridge spans:

1) Joints at mid-span,
2) Joints at a pier in continuous-span or cantilevered truss construction,
3) Joints near a pier in continuous-span or cantilevered truss construction,
4) Joints at an inflection point in continuous-span or cantilevered truss construction,
5) 90 degree angle corner joints at the simply-supported end of a span,
6) Top chord corner joints with a larger than 90 degree angle between the chord and the end diagonal member at the simply-supported end of a span, and
7) Bottom chord joints at the start of a haunch over an interior pier in continuous-span or cantilevered truss construction.

Based on the above locations, a total of 20 configurations were designed. By considering mid-span, pier, near pier and inflection point locations, the geometry conditions and force demands at the test joint can be varied substantially. The location of a joint in a given bridge span has a significant influence on the ratio of the vertical shear versus the major-axis bending moment resisted by the truss. In addition, the depth of the truss impacts the chord forces given the truss major-axis bending moment. Also, the orientation of the diagonals impacts the magnitude of the shear force transferred by the gusset plates parallel to the line of the chords, which develops the chord forces. The orientation of the diagonals is of course determined by the ratio of the truss depth to the truss panel length along the span. White et al. (2013) provides the detailed force demands for the 20 representative configurations. Figure 1 shows the Warren with vertical configurations with reference applied loadings corresponding to items (1) to (4) in the above list. The circles in Fig. 1 highlight the location of the joint under study. In this paper, analysis results for Case P5 and several variations on this case are discussed in detail.

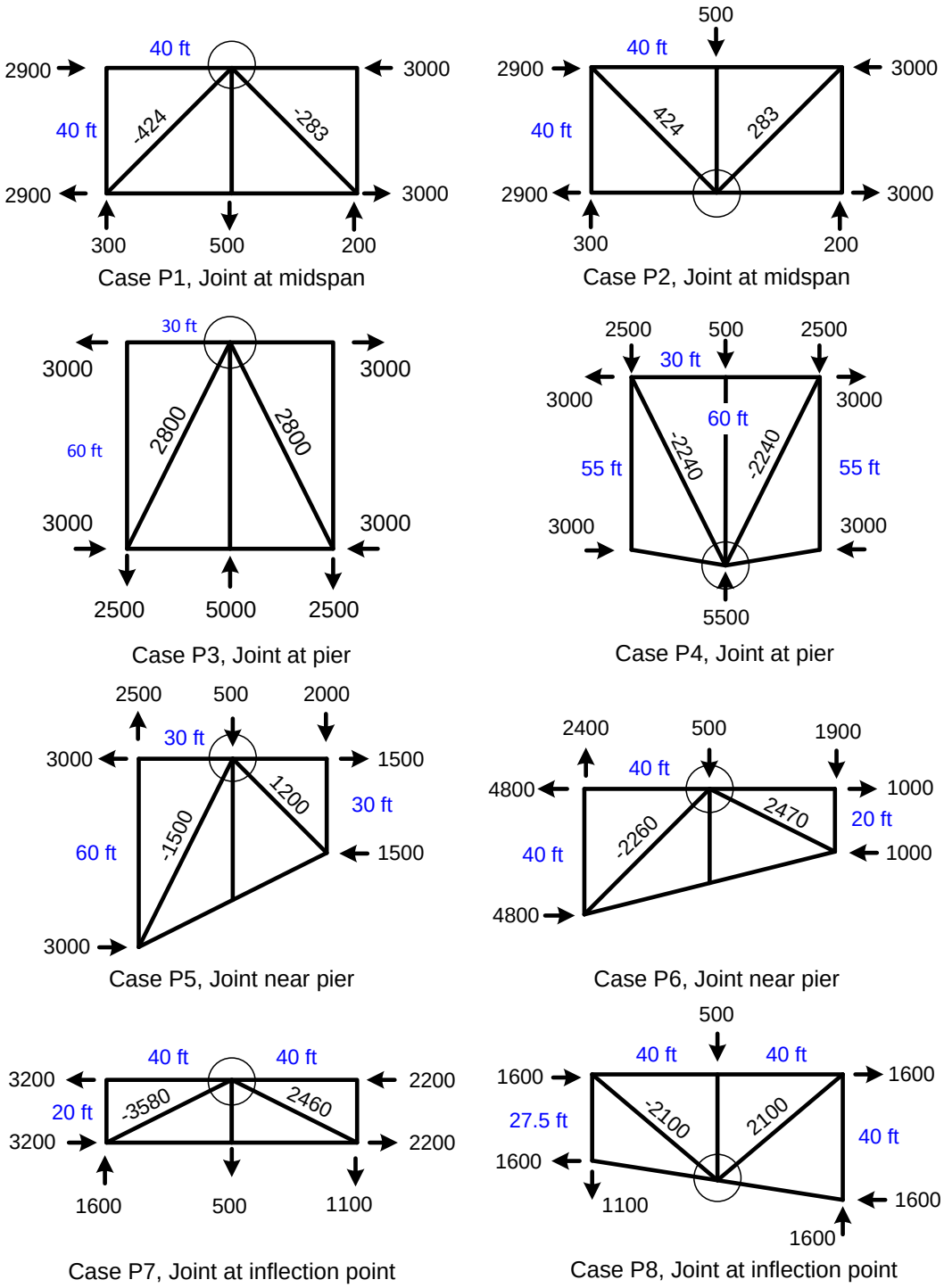

Figure 1: Warren truss with vertical member configurations (all loads are in kips).

2.2 Joint Parameters

The key parameters selected to investigate the behavior of gusset plate joints were:

1) Mill to bear versus non-mill to bear compression splices
2) Material strength
3) Member chamfer versus no member chamfer
4) Shingle plates
5) Edge stiffening
6) Corrosion

In this paper, the effect of member chamfer is discussed using Case P5 shown in Fig. 1.

2.2 Joint Design

To design the test joints, five box-sections and three I-sections were designed first to resist the ranges of compression and tension forces obtained from the subassembly geometries. Based on the available bridge plans of longer Warren trusses with verticals, it was decided to keep the out-of-plane dimension constant at 21 inches. Using the selected joint configurations and member cross-sections, the initial set of 20 parametric study gusset plate joints was designed. Subsequently, additional gusset plate joints were studied by varying the parameters discussed above. In general, several design rules were used to ensure reasonable joint sizes and efficient designs. These rules were:

1) The centerlines of the members always intersect at a common work point.
2) The minimum clearance between the members is 1 inch.
3) All the connections have a minimum of six rows of fasteners along the member length.
4) The chord members have the same cross-section on each side of the test joint.
5) The truss chords are spliced at the joint work point.
6) Web splice plates are attached inside the chord members at the joint; additional splice plates are attached to the outside of the chord members at the top and bottom flanges.
7) The geometry of the splice plates is symmetric about the work point at a given joint.
8) Chamfered members have at least two fasteners in the last row at the end of the member.
9) The fasteners are all 7/8 inch diameter.
10) A spacing and pitch of 3 inches and an edge distance of 1.5 inches is used to lay out a rectangular grid of fasteners within each connection. Fasteners are removed from selected locations within the rectangular grids to reduce the total number of fasteners where the additional capacity is not needed.
11) The maximum edge distance of the connection blocks is approximately 2.5 inches.

Figure 2 shows a typical joint design considered in this research. This is Case P5-C-WV-NP, which is discussed below. For the initial 20 designs, all the diagonals were chamfered as much as possible. A number of the joints were then re-designed without chamfer and studied.

3. Test Simulation Procedures

Figure 3 shows a typical test simulation model used in the current research. In all subsequent discussions, the joints in these two-panel subassemblies are always referred to as U_1 through U_3

on the upper chords and L_1 through L_3 on the lower chords. In all cases, the gusset plate test joint is located either at the U_2 or L_2 location. The test simulations were performed using Abaqus (Simulia 2010). In all the cases, the gusset plates, splice plates, and the portion of the members in the vicinity of the test joint are modeled using four-node shell elements referred to as the S4R element in Abaqus. All the parts in Fig. 3 not shown as lines are modeled using S4R elements. The remaining lengths of the truss members, as well as the other truss members not connected to the gusset plate joints, are modeled using 2-node B31 beam elements. Multi-point constraints are used to connect the member cross-section modeled with shell elements to the corresponding end node of a beam element at the transition between the element types.

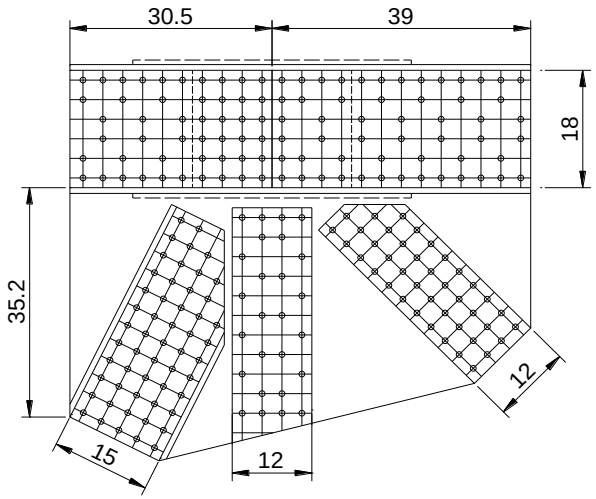

Figure 2: Typical joint configuration (Case P5-C-WV-NP, all dimensions are in inches)

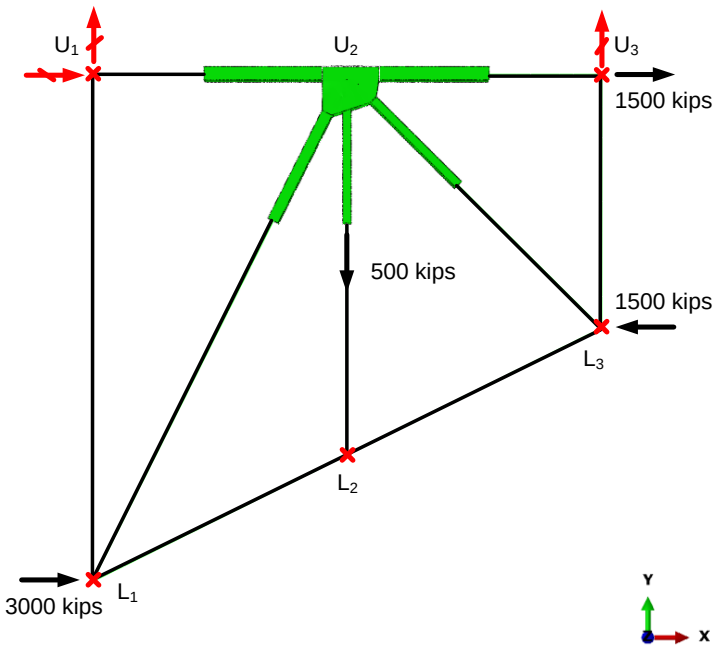

Figure 3: Typical test simulation model with loadings and boundary conditions (Case P5-C-WV-NP)

Figure 3 also shows typical loading and boundary conditions used in this research. All the end nodes of the truss members on the outside perimeter of two-panel system (L_1 to L_3, U_1, and U_3 in Fig. 3) are restrained in the out-of-plane direction. For in-plane movements, a simply supported condition is modeled. For the case shown in Fig. 3, horizontal and vertical displacements are restrained at U_1 and the vertical displacement is restrained at U_3. In addition, an out-of-plane restraint is applied at one node at the center of the top or bottom splice plates at the test joint, whichever is on the outside of the joint, to prevent overall out-of-plane movement of the test joint. The reaction due to this restraint was found to be small in all the study joints.

As shown in Fig. 3, loads are applied at the nodes at the left and right end of the two-panel system (L_1, L_3, U_1, and U_3 in this figure) except for the 500-kip load applied at the vertical member. Whenever there is a load applied at the truss cross-section corresponding to the test joint, this load was applied at the location where the shell-element cross-section is attached by a multi-point constraint to the beam element model. This decision was based on the fact that in actual bridges, this load is transferred typically from a floor beam which is attached at some location away from the joint. By applying this load at the end node of a beam element, any issues associated with stress concentrations from a point load applied to the shell elements are avoided.

Figure 4 shows typical geometric imperfection shapes used in the simulations. It can be seen that geometric imperfections are incorporated not only into the gusset plates but also in the compression diagonal (the left diagonal member). These imperfections were generated by separate linear elastic analyses in which pressure loads were applied on the gusset plates to generate an out-of-flatness of the gusset plates on the compression diagonal side. In addition, out-of-plane displacements were applied at the end of the compression diagonal so that an initial out-of-alignment of the member was also generated. These deformations were scaled so that the gusset plate out-of-flatness is $L_{max}/150$, where L_{max} is the maximum free-edge length, and the out-of-alignment of the diagonal matches $0.1L_{gap}$, where L_{gap} is the smallest length of the gap between the compression diagonal and the adjacent members. Various early studies demonstrated that the gusset plate maximum strength is not sensitive to the imperfection magnitude or pattern once initial imperfections that are a small fraction of the above tolerances are applied.

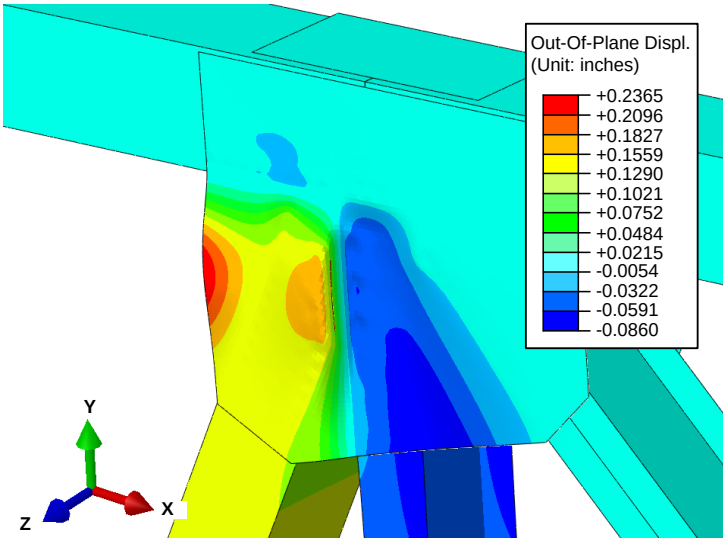

Figure 4: Typical geometric imperfection shape

Figure 5 shows the true stress-strain curves for Grade 50 and Grade 100 steel used in the test simulations. These curves were established from tension coupon test data and are representative expected curves for these types of materials. Abaqus assumes a flat plateau after the end point of the true stress-strain responses shown in Fig. 5. Generally, this is beyond the maximum strain required for assessment of the joint behavior.

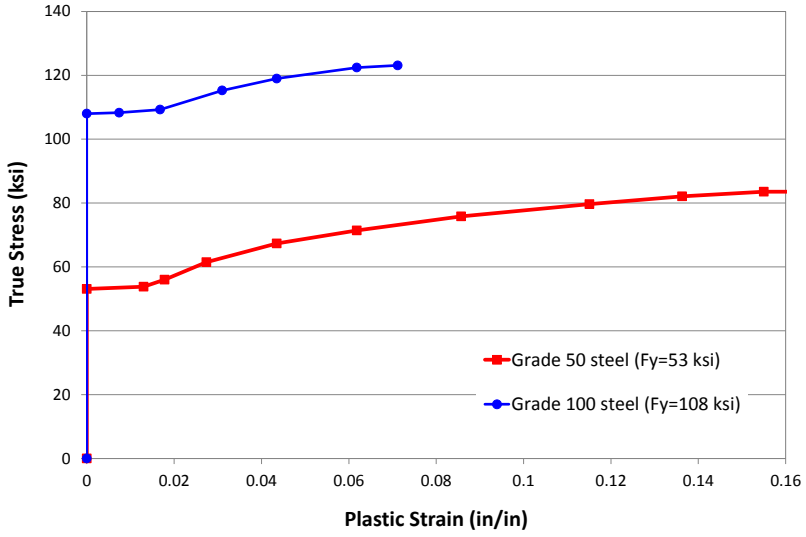

Figure 5: True stress-strain curve for Grade 50 steel

For all the test simulations, the fasteners are modeled explicitly using nonlinear force-shear deformation relationships using connector elements in Abaqus. Figure 6 shows the nonlinear shear force-displacement curves for hot driven rivets. The fastener properties are modeled such that the strength curves shown in Fig. 6 are applied to the resultant of the shear loads within the fastener element. For the places where fasteners connect three or more plates, the fasteners have two or more layers of connector elements. For the out-of-plane component for the fastener force-deformation response (i.e., the fastener axial tension force-elongation response), elastic behavior is assumed with a stiffness of EA/L, where E is Young's modulus, A is the area of the fastener shank, and L is the total length of the fastener. The relative movements between the ends of the connector elements (located at the mid-thickness of the plates) are modeled such that relative rotation of the plates is restrained but the relative plate displacements are allowed. Early project studies showed that the joint response is insensitive to the fastener type, if the different fastener types are used with the same connection geometry (of course, different fastener design resistances can lead to significantly different connection sizes and geometries).

To evaluate the finite element simulation procedures used in this research, full-scale experimental tests were analyzed using the above methodology and the corresponding simulation results were compared with the experimental response. Shown below are the simulation results from Specimen E4-U-490SS-WV. This specimen had unchamfered members, A490 high-strength bolts, a short standoff distance (1.0 inch) for the compression diagonal, and a short connection length to the compression diagonal. Figure 7(a) shows key dimensions of this joint. It should be noted that a minimum fastener spacing of 2.5 inches and an edge distance of 1.5 inches is used in this test. Figure 7(b) shows the member forces at the maximum load obtained in the experiment. These forces are applied as reference loads in the test simulation.

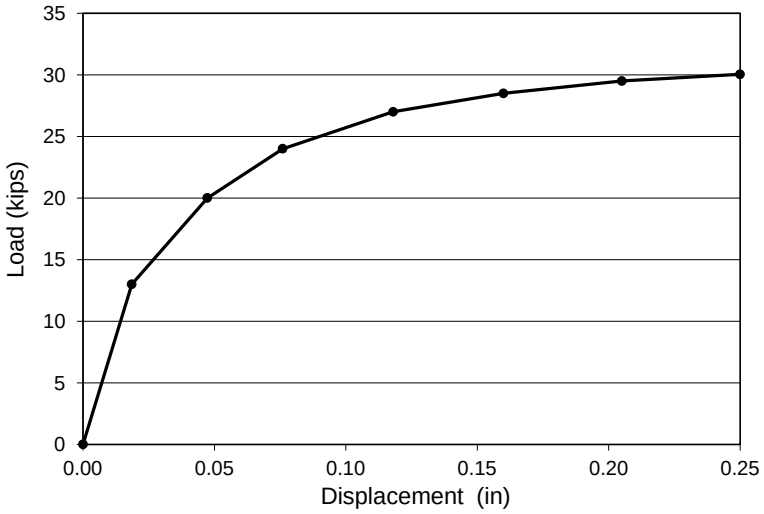

Figure 6: Nonlinear shear-force shear-displacement curve for hot driven rivets in single shear.

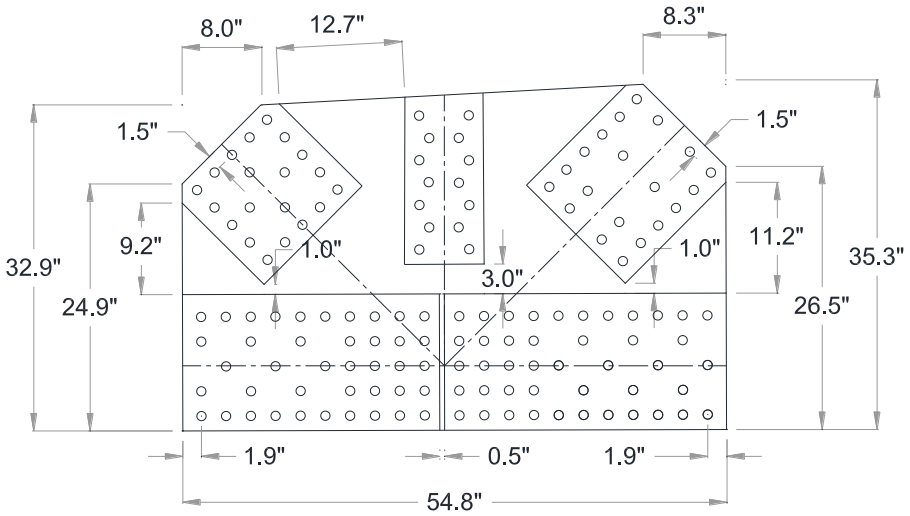

(a) Gusset plate geometry

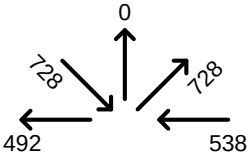

(b) Member forces at the maximum load obtained in the experiment

Figure 7: Gusset plate geometry and member forces at the maximum experimental load for E4-U-490SS-WV.

Figure 8 shows in-plane and out-of-plane displacements versus the applied load fraction (ALF) for E4-U-490SS-WV with a gusset thickness of 3/8 inches. These plots indicate that the joint has reached its limit load at 1.04 times the experimental failure load (ALF = 1.04) and that the failure mode involves in-plane as well as out-of-plane movements of the compression diagonal. Figure 9 shows Tresca strains from digital image correlation obtained from the experimental test and from the analysis simulation of the specimen approximately at ALF = 1.0. One can observe that the

analysis simulation results capture the overall responses of the experimental results closely although slight differences in the strain contours exist at the end of the compression diagonal and along the horizontal region above the chord members. The reader is referred to Mentes (2011) for a thorough discussion the experimental and simulation results for this and other tests.

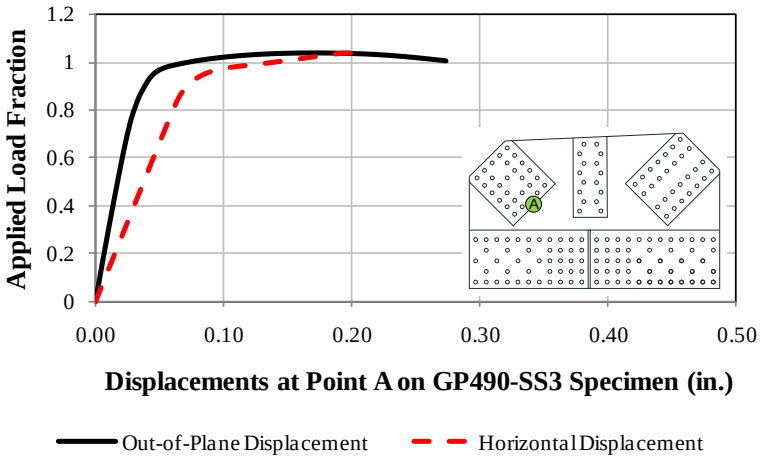

Figure 8: In-plane vs. out-of-plane displacement of E4-U-490SS-WV from the test simulation.

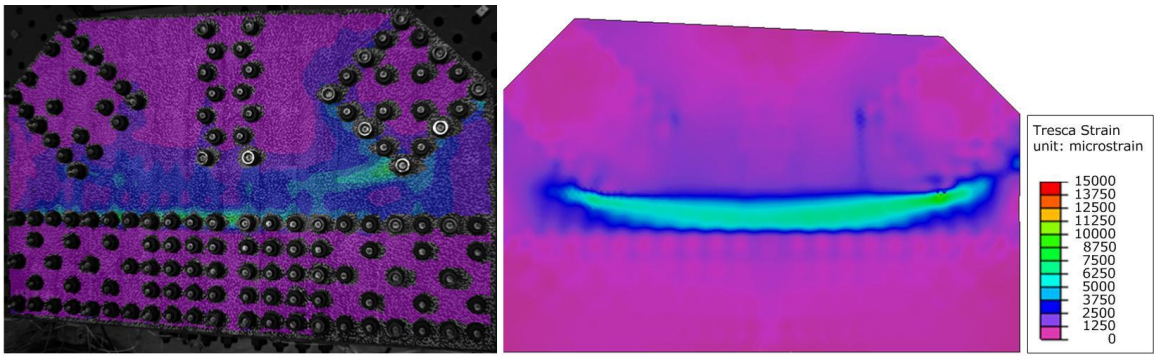

Figure 9: Tresca strains obtained from the digital image correlation (left) and analysis simulation (right) at approximately ALF = 1.0 (Mentes 2011).

4. Test Simulation Results

In the finite element analyses conducted in this research, the maximum load capacity for the test specimens is defined as the load level at which a test first reaches:

(1) 4% equivalent plastic strain (PEEQ) over a length equal to the plate thickness at the mid-surface of any of the plates (gusset, shingle, and splice), or

(2) The peak load on the load-displacement curve.

The 4% PEEQ criterion is a somewhat arbitrary limit beyond which potential rupture of the physical material may become suspect. This is also a limit commonly used in the published literature at which the strains are considered as "large." In general, the 4% criterion governed in situations that failed in a shear-deformation dominant failure mode. The peak load criterion is a natural choice for buckling-dominated behavior, where extensive unloading occurs as the loading progresses. In cases where a specimen may unload and subsequently continue to support greater

loads, the first peak was chosen as the failure load. In some cases, post-buckling strength causes some subsequent increases in the load capacity, but this occurs at relatively large deformations.

4.1 P5-C-WV-NP and P5-U-WV-NP

Joint P5-C-WV-NP is an upper-chord joint with chamfered members located near a pier of a continuous Warren truss bridge with vertical members. Figure 2 shows key dimensions of the gusset plate and its members for Case P5-C-WV-NP and Fig. 10 shows the corresponding reference member forces. The configuration of the test subassembly with applied loadings and boundary conditions is shown in Fig. 3. As can be seen from Figs. 3 and 10, the compression diagonal is relatively steep. The 3000 and 1500 kip tension forces in the chord cause significant shear stress across the horizontal plane of the gusset, while the compression diagonal force of 1500 kips causes significant gusset plate compression stresses.

To investigate the effect of member chamfer on the joint behavior, P5-C-WV-NP is modified such that the diagonal members are not chamfered. This case is labeled P5-U-WV-NP and is shown in Fig. 11. Since the members are unchamfered, the gusset plate of P5-U-WV-NP has a significantly longer vertical free edge between the top left chord member and the compression diagonal. The joint configuration and applied loading and boundary conditions for P5-U-WV-NP are the same as P5-C-WV-NP.

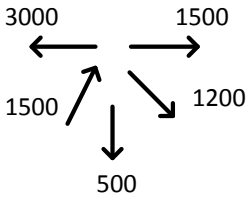

Figure 10. Design forces for P5-C-WV-NP and P5-U-WV-NP.

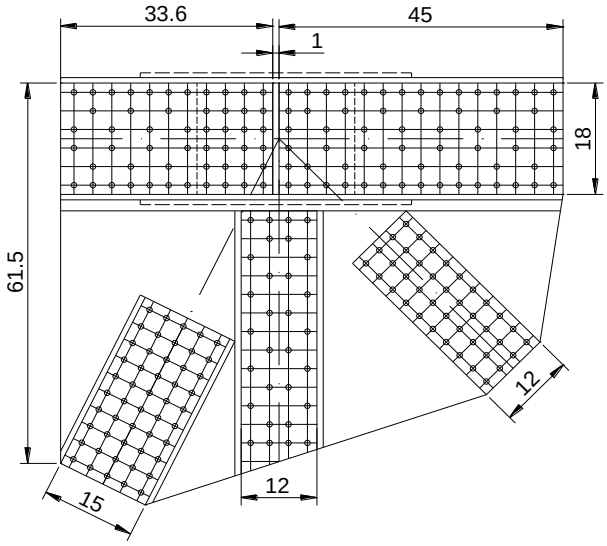

Figure 11. Gusset plate geometry for P5-U-WV-NP (unit = inches).

Table 1 lists the required gusset thicknesses obtained using adaptations of the FHWA Guide for the given loading conditions. For P5-C-WV-NP, *Whitmore buckling* of the compression diagonal

required a gusset thickness of 0.34 inches calculated with $K = 0$. It should be noted that the FHWA Guide recommends using $K = 1.2$ for sway buckling. However, it was decided to assume the full yield strength for the cases where the members are chamfered, i.e., $K = 0$, in the test joint designs. The shear checks of the horizontal and vertical planes required a 0.40 and 0.43 inch gusset plate respectively. A gusset thickness of 0.4 inches, splice plate thicknesses of 0.78 inches on the outside of the chord flanges, and a web splice plate thicknesses inside the chord of 0.51 inches were selected for the simulation presented below.

Table 1 also gives the gusset plate thickness requirements for P5-U-WV-NP based on adaptations of the FHWA Guide. As expected, the edge slenderness check required significantly thicker gusset plates in this test because of the long vertical edge between the chord and compression diagonal members. For the gusset of P5-U-WV-NP, $K = 1.2$ was used to calculate the *Whitmore buckling* resistance at the compression diagonal. This check required a gusset thickness of 0.65 inches. The shear checks of the horizontal and vertical planes of P5-U-WV-NP were less critical; the required gusset plate thicknesses were 0.38 and 0.35 inches respectively for these limit states (using $\Omega = 1$). For the FEA test simulation below, a gusset thickness of 0.40 inches was selected, which is same as the base thickness used in P5-C-WV-NP.

Table 1. Required gusset plate thicknesses from the FHWA Guide for P5-U-WV-NP.

Limit State	$t_{g.req}$ (in)	
	P5-U	P5-C
Edge slenderness check on compression diagonal side	0.89	0.73
Whitmore buckling at compression diagonal	0.65 ($K = 1.2$)	0.34 ($K = 0$)
Block shear rupture at tension diagonal	0.41	0.40
Tension rupture check for the left chord	0.40	0.43
Vertical plane shear along left side of vertical	0.38 ($\Omega = 1$)	0.43 ($\Omega = 1$)
Horizontal plane shear along chords	0.35 ($\Omega = 1$)	0.40 ($\Omega = 1$)

Figure 12 shows a load-displacement plot for P5-C(0.4)-WV-NP. The number shown inside a parenthesis (0.4) indicates the selected gusset plate thickness in the following discussions throughout the paper. In Fig. 12, the abscissa is the vertical deflection at U_2. Figure 12 shows that the P5-C(0.4)-WV-NP configuration reaches its load capacity at an ALF of 0.94 (at the first peak), based on the limit load criterion. While the ALF subsequently reaches above 1.00, this value was not taken as the strength since it required the development of large deformations.

Figures 13 and 14 show the von Mises stress and equivalent plastic strain contours at the limit load in this test using a deformation scale factor (DSF) of 5. The equivalent plastic strain contours in Fig. 14 show extensive yielding around the entire periphery of the compression diagonal at the strength limit, with the largest concentration of plastic strain occurring at the chamfered and non-chamfered ends of the compression diagonal. In addition, out-of-plane movement of the compression diagonal and of the long free edge of the gusset plate is evident at the strength limit. Figure 15 shows the variation of the normal, shear and von Mises stresses on the vertical plane at the edge of the vertical member on the compression diagonal side of the gusset. One can observe that the gusset plate is essentially fully yielded in shear except for where it is bolted to the truss chord. Figure 16 illustrates the variation of the shear stress on the horizontal plane just below the chord. This plane is also nearly fully yielded, but there is significant interaction between the normal and shear stresses in the vicinity of the small offset of the compression diagonal from the chord.

Figure 17 shows a load-displacement plot for P5-U(0.4)-WV-NP. The abscissa is the vertical deflection at U_2, as in the Fig. 12 for P5-C(0.4)-WV-NP. This plot shows that the P5-U(0.4)-WV-NP joint reaches its limit load at an ALF of 0.78 whereas an ALF of 0.94 is reached for P5-C(0.4)-WV-NP. For P5-C(0.4)-WV-NP and P5-U(0.4)-WV-NP, the maximum PEEQ is 2 % and 0.4 % respectively at the limit load.

Figure 18 shows the equivalent plastic strain contours for P5-U(0.4)-WV-NP at the limit load for this problem, using a displacement scale factor (DSF) of 5 on the deformed geometry. These contours show the gusset plates are yielded slightly within the area below the top left chord member and at the end of the compression diagonal. Also, the vertical free edge between the top chord and compression diagonal member is buckled out-of-plane.

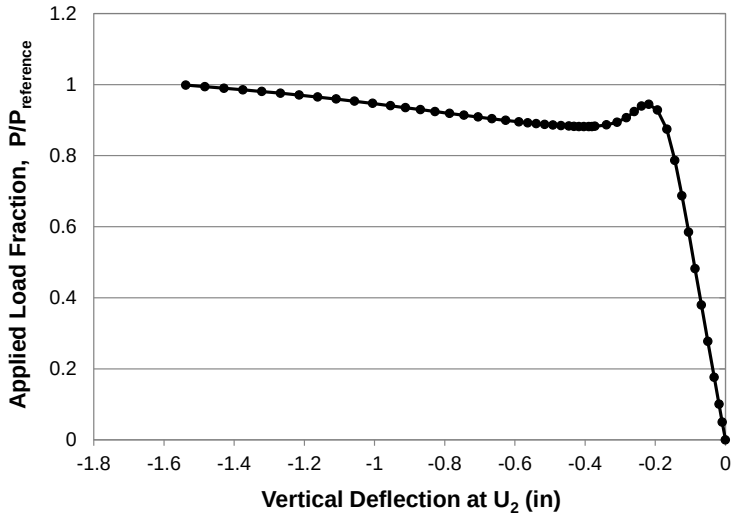

Figure 12. Load-displacement plot for P5-C(0.4)-WV-NP.

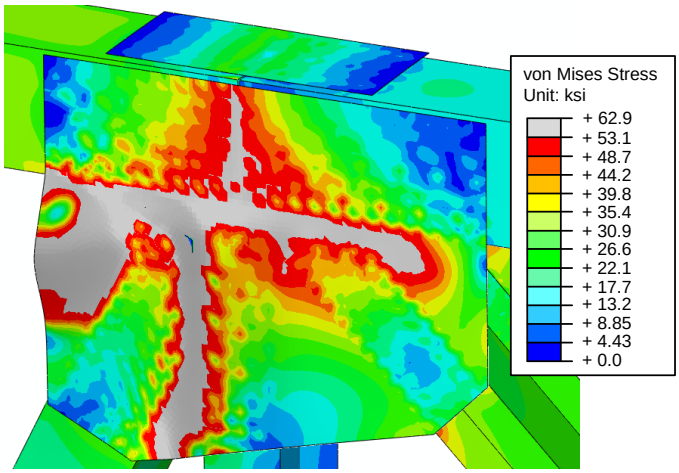

Figure 13. von Mises stress contours for P5-C(0.4)-WV-NP at the limit load occurring at an ALF of 0.94 (DSF = 5).

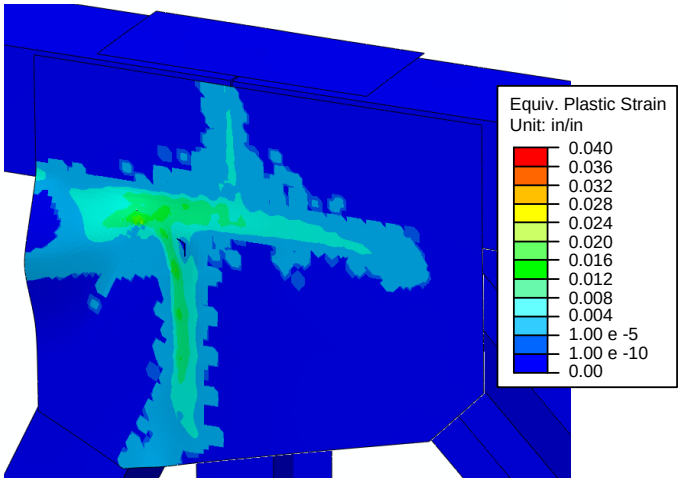

Figure 14. Equivalent plastic strain contours for P5-C(0.4)-WV-NP at the limit load occurring at an ALF of 0.94 (DSF = 5).

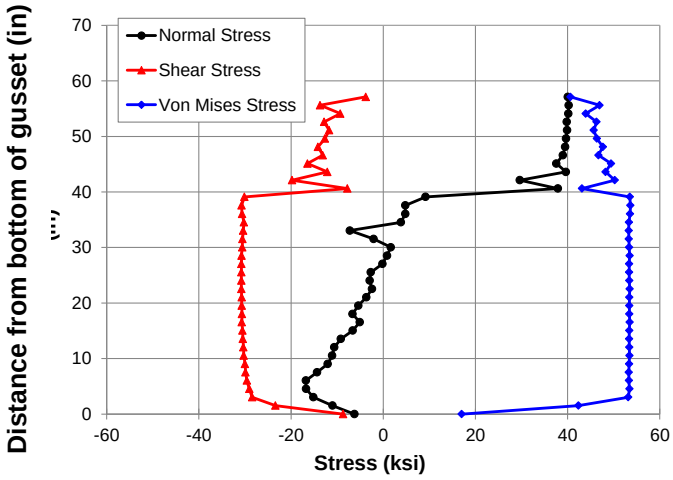

Figure 15. von Mises, normal, and shear stresses along the vertical plane of P5-C(0.4)-WV-NP at the limit load occurring at an ALF of 0.94.

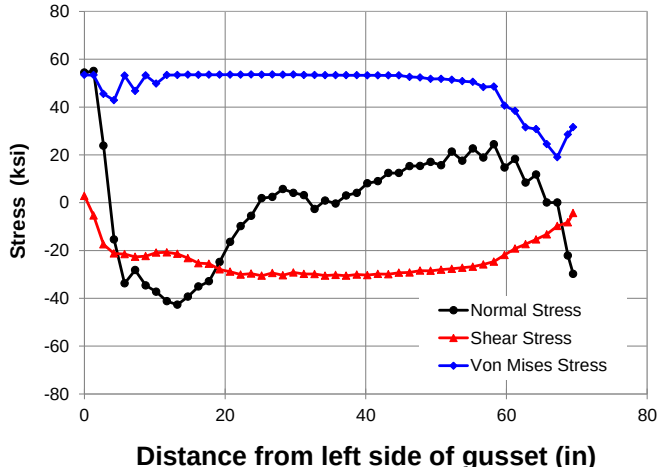

Figure 16. von Mises, normal, and shear stresses along the horizontal plane of P5-C(0.4)-WV-NP at the limit load occurring at an ALF of 0.94.

In this problem, the compression diagonal starts moving out-of-plane significantly just after significant out-of-plane movement of the free edge occurs. Figure 19 shows the equivalent plastic strain contours on the deformed geometry of the joint (DSF = 5) within the post-peak range of the response (at ALF = 0.55). These contours show significant out-of-plane sway buckling of the gusset plate. The thickness t_g = 0.4 is substantially smaller than required by the FHWA Guide for edge slenderness and *Whitmore buckling* strength along the compression diagonal, corresponding to $t_{g.req}$ = 0.65 and 0.89 respectively (see Table 1). When the gusset plate thickness is increased to 0.5 inches, the peak ALF increases to 1.09 (corresponding simulation results not shown). This indicates that the edge slenderness check and the *Whitmore buckling* calculation with K = 1.2 are significantly conservative for P5-U(0.4)-WV-NP.

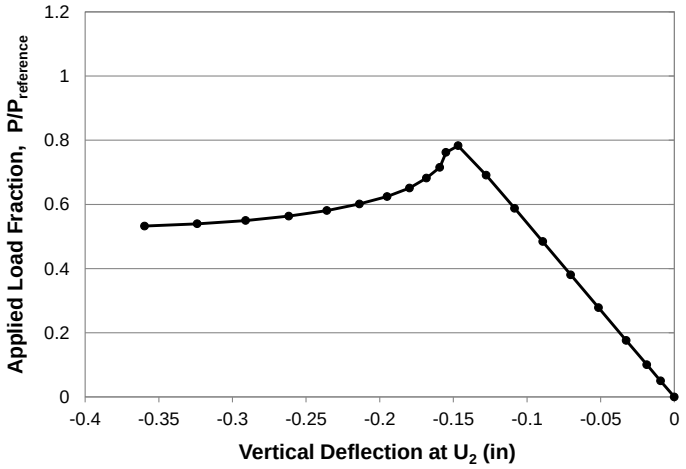

Figure 17. Load-displacement plot for P5-U(0.4)-WV-NP.

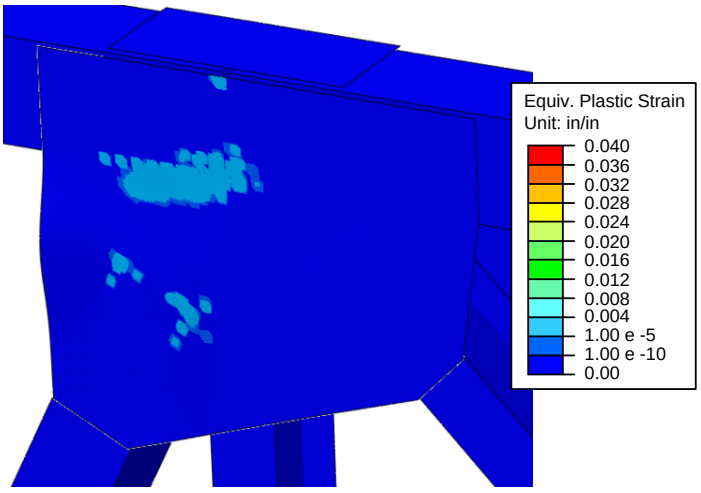

Figure 18. Equivalent plastic strain contours for P5-U(0.4)-WV-NP at the limit load occurring at an ALF of 0.78 (DSF = 5).

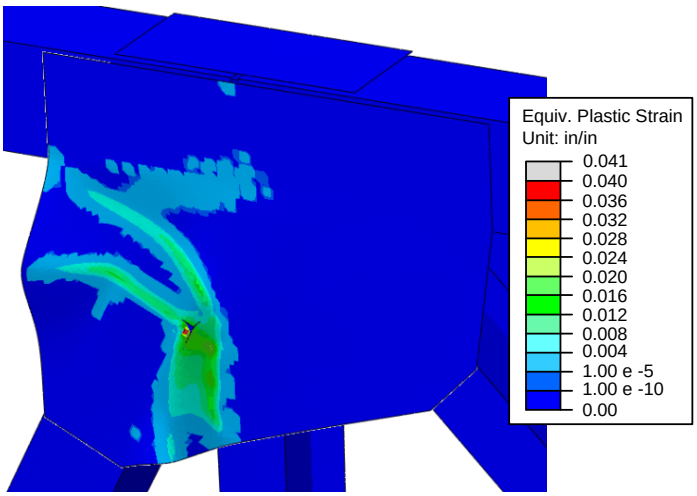

Figure 19. Equivalent plastic strain contours for P5-U(0.4)-WV-NP at a post-peak ALF of 0.55 (DSF = 5).

5. Design Recommendations for Diagonal Buckling

Based on the simulation results conducted in this research, a number of design recommendations have been proposed. In this paper, recommendations for checking the gusset plate diagonal buckling resistance are discussed. For other recommendations, the reader is referred to White et al. (2013) and FHWA (2013). It should be noted that two methods (*Method 1* and *Method 2*) are proposed from this research. The *Method 1* procedures are simpler, but are somewhat less accurate in their characterization of the gusset-plate resistances. A version of Method 1 has been proposed for adoption by the AASHTO Specifications. The following sections discuss the *Method 1* and *Method 2* approaches for evaluating buckling of a gusset plate in the vicinity of a compression diagonal

5.1 Diagonal Buckling, Method 1: Whitmore Section and Separate Partial Shear Plane Failure Checks

In general, the *Method 1* procedure determines diagonal buckling strength using the full Whitmore section and the average "column" lengths measured from the both ends and middle of the Whitmore section to adjacent fastener lines. To define the Whitmore section, one needs to draw a line along the last row of fasteners in the compressive diagonal connection. The width along this line bounded by two lines that fan out at 30 degrees from the outside fasteners at the opposite end of the connection is the full Whitmore section width. The full Whitmore section is calculated as

$$W_{Whitmore} = W_{conn} + 2\, L_{conn} \tan(30) \quad (1)$$

For cases where a diagonal is heavily chamfered or has significantly smaller offset to the adjacent members, the full width of the Whitmore section can extend outside the free edges of the gusset plates or planes of symmetry within the joint. In these cases, the Whitmore section should be truncated at the intersections with free edges of the gusset plate and at planes of symmetry; however, otherwise, the full Whitmore section is used regardless of the intersections with adjacent fastener lines or intersections with the Whitmore section of adjacent members in *Method 1*. For the compression diagonal of Case P5-C-WV-NP, the full width of the Whitmore section exceeds the left free edge of the gusset plate by 0.4 inches. Therefore, the truncated

Whitmore width ($W_{Whitmore}$ = 49.7 inches) is used for the strength calculations rather than the full Whitmore width. Figure 20 shows the truncated Whitmore section of Case P5-C-WV-NP

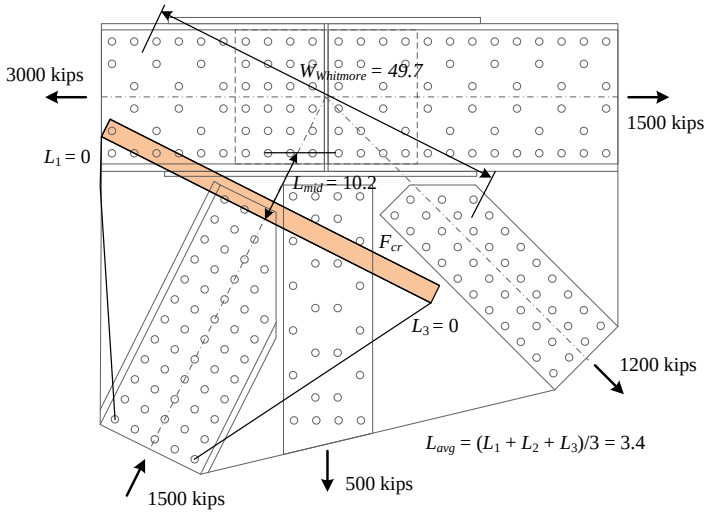

Figure 20. *Method 1* Gusset plate diagonal buckling model with truncated Whitmore section, shown on P5-C-WV-NP.

Once the Whitmore width is determined, the *Method 1* diagonal buckling strength is calculated as

$$\begin{aligned} P_{n.Whitmore} &= 0.658^{F_y/F_e} F_y A_g \quad \text{if} \quad F_y/F_e \le 2.25 \\ &= 0.877 F_e A_g \qquad \text{otherwise} \end{aligned} \tag{2}$$

where

$$F_e = \frac{\pi^2 E}{(KL_{avg}/r)^2} = \frac{3.29E}{(L_{avg}/t_g)^2} \tag{3}$$

$$K = 0.5 \tag{4}$$

$$r = \frac{t_g}{\sqrt{12}} \tag{5}$$

$$A_g = 2W_{Whitmore}\, t_g \tag{6}$$

When the buckling strength check is performed, one should also check the shear strengths of the partial shear planes next to the diagonal. The research observed that in numerous cases, a compression failure could be triggered by the onset of shear yielding along such planes. The partial shear plane that controls is the one that:

- Parallels the chamfer in the compression diagonal, for cases where only one side of the compression diagonal is chamfered,
- Has the smaller framing angle between the compression diagonal and the adjacent members, or
- Has the shortest length if the compression diagonal is unchamfered and the framing angles with the adjacent members are equal.

Figure 21 shows the length of partial shear plane for P5-U-WV-NP. The partial shear plane strength is determined as

$$P_{n.PartialShear} = \frac{2\left(0.58F_y L_{PartialShear} t_g\right)}{\cos\theta} \tag{7}$$

Then the nominal strength of diagonal buckling is determined as

$$P_n = \min(P_{n.Whitmore}, P_{n.PartialShear}) \tag{8}$$

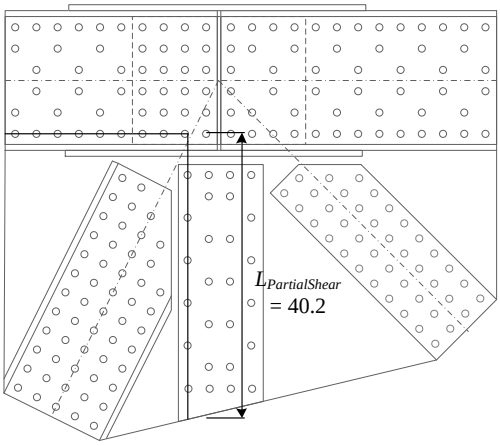

Figure 21. *Method 1* Partial shear planes on P5-C-WV-NP.

The *Method 1* calculation of the diagonal buckling strength for P5-C(0.4)-WV-NP is thus:

F_y = 53 ksi

$W_{Whitmore}$ = 49.7 in

A_g = 2 x 49.7 x 0.4 = 39.8 in^2

L_{avg} = (0 + 10.2 + 0)/3 = 3.4 in

$$F_e = \frac{3.29 \times 29{,}000}{(3.4/0.4)^2} = 1321 \text{ ksi}$$

$$\frac{F_y}{F_e} = \frac{53}{1321} = 0.004$$

$$P_n = 0.658^{0.004} \times 53 \times 34.6 = 0.998 \times 53 \times 39.8 = 2106 \text{ kips}$$

$L_{PartialShear}$ = 40.2 in

$$P_{n.PartialShear} = \frac{2 \times 0.58 \times 53 \times 40.2 \times 0.4}{\cos(26.6)} = 1106 \text{ kips}$$

P_n = min(2106, 1106) = 1106 kips

P_{test} = 0.94 x 1500 = 1410 kips

P_{test}/P_n = 1410/1106 = 1.27

5.2 Diagonal Buckling, Method 2: Truncated Whitmore Section

In cases where a diagonal is heavily chamfered, the Whitmore section can easily extend beyond the fastener lines of adjacent members. In the *Method 2* "truncated Whitmore section" approach, it is assumed that the compressive stresses transferred from the compression diagonal are distributed along the adjacent fastener lines. To estimate the buckling strength of the gusset plate along these fastener lines, a column analogy is used with a column width being a width of the adjacent fastener lines projected onto the Whitmore section and a column length measured from the external fastener lines of the connection to the adjacent fastener lines. Figure 22 shows an example of the *Method 2* truncated Whitmore section and assumed stress distributions on Case P5-C-WV-NP. In Fig. 22, one can observe that the column length of the middle width L_M is measured at the *middle* of W_M. Figure 22 also shows that on the left and right widths W_L and W_R, a 90 % of the column buckling strength F_{cr} is assumed to be developed.

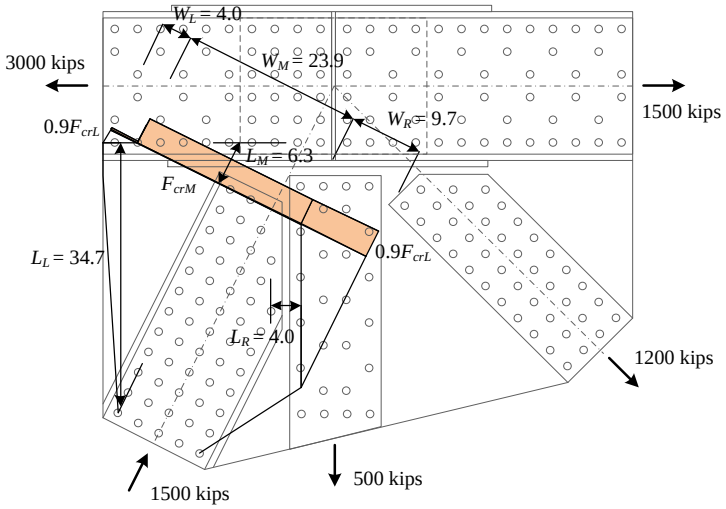

Figure 22. *Method 2* gusset plate diagonal buckling model with truncated Whitmore section, for P5-C-WV-NP .

The *Method 2* diagonal buckling strength is calculated as follows:

(1) For the middle widths W_M, determine P_n as

$$\begin{aligned} P_{nM} &= 0.658^{F_y/F_e} F_y A_g \quad \text{if} \quad F_y/F_e \le 2.25 \\ &= 0.877 F_e A_g \qquad \text{otherwise} \end{aligned} \tag{9}$$

where

$$F_e = \frac{\pi^2 E}{(KL_M/r)^2} = \frac{3.29E}{(L_M/t_g)^2} \tag{10}$$

$$K = 0.35 \tag{11}$$

$$r = \frac{t_g}{\sqrt{12}} \tag{12}$$

$$A_g = 2W_M t_g \tag{13}$$

(2) For the left and right widths W_L and W_R, determine P_n as

$$P_{nL,R} = 0.9 \times 0.658^{F_y / F_e} F_y A_g \quad \text{if} \quad F_y / F_e \le 2.25$$
$$= 0.9 \times 0.877 F_e A_g \qquad \text{otherwise} \tag{14}$$

where F_e, K, r, and A_g are calculated using Eqs. (9) to (13) using the corresponding column length and width.

(3) The buckling strength of the *Method 2* truncated Whitmore section is calculated as

$$P_n = P_{nL} + P_{nM} + P_{nR} \tag{14}$$

The calculation of the diagonal buckling strength using the *Method* 2 truncated Whitmore section for P5-C(0.4)-WV-NP is shown below:

F_y = 53 ksi

W_L = 4.0 in; L_L = 34.7; $F_{eL} = \dfrac{6.71 \times 29{,}000}{(34.7/0.4)^2} = 25.9$ ksi; $\dfrac{F_y}{F_{eL}} = \dfrac{53}{25.9} = 2.05$

$P_{nL} = 2 \times \left(0.9 \times 0.658^{2.05} \times 53 \times 4.0 \times 0.2\right) = 64.7$ kips

W_R = 9.7 in; L_R = 4.0; $F_{eR} = \dfrac{6.71 \times 29{,}000}{(4.0/0.4)^2} = 1946$ ksi; $\dfrac{F_y}{F_{eR}} = \dfrac{53}{1946} = 0.027$

$P_{nR} = 2 \times \left(0.9 \times 0.658^{0.027} \times 53 \times 9.7 \times 0.4\right) = 2 \times \left(0.989 \times 53 \times 3.88\right) = 366$ kips

W_M = 23.9 in; L_M = 6.3; $F_{eM} = \dfrac{6.71 \times 29{,}000}{(6.3/0.4)^2} = 784$ ksi; $\dfrac{F_y}{F_{eM}} = \dfrac{53}{784} = 0.068$

$P_{nM} = 2 \times \left(0.658^{0.068} \times 53 \times 23.9 \times 0.4\right) = 2 \times \left(0.972 \times 53 \times 9.56\right) = 985$kips

$P_n = P_{nL} + P_{nR} + P_{nM}$ = 64.7 + 366 + 985 = 1416 kips

P_{test} = 0.94 x 1500 = 1410 kips

P_{test}/P_n = 1410/1416 = 1.00

5.3. Assessment of Method 1 and Method 2 Diagonal Buckling Checks

From the example *Method 1* and *Method 2* calculations shown above, one can observe that the *Method 1* procedure is simpler but provides a less accurate estimation in terms of gusset plate resistances. Especially for the cases where the diagonals are heavily chamfered and the Whitmore width overlaps significantly with the adjacent members such as Case P5-C-WV-NP, the *Method 1* procedure tends to provide conservative results. Table 2 shows a summary assessment of the *Method 1* and *Method 2* procedures determined based on 63 parametric tests. The mean professional factor P_{test}/P_n of the two procedures are close. However, *Method 2* exhibits a smaller coefficient of variation and a significantly larger minimum value of P_{test}/P_n.

Table 2. Summary assessment of *Method 1* and *Method 2* prediction equations for diagonal buckling, 63 parametric tests.

	Method 1	*Method 2*
Mean	1.08	1.06
Standard Deviation	0.19	0.11
Coefficient of Variation	0.18	0.10
Maximum	1.43	1.29
Minimum	0.61	0.86

Conclusions

This paper discusses analytical research conducted at Georgia Institute of Technology in support of NCHRP 12-84, with emphasis on findings pertinent to the compressive resistance of gusset plates at compression diagonals. Representative cases showing with chamfered and non-chamfered member geometries are selected and the corresponding results are discussed. Proposed design calculations for estimating diagonal buckling strengths of gusset plates are discussed and calculation examples are presented using the test cases discussed in the paper.

Acknowledgments

This work was sponsored by the Federal Highway Administration and was conducted in support of the National Cooperative Highway Research Program (NCHRP) project 12-84. The authors are grateful for the input and advice from the NCHRP panel overseeing this broad research project. Special thanks are extended to Justin M. Ocel and Robert S. Zobel of FHWA for extensive discussions, feedback, and collaboration during the analytical studies as well as their skillful management of the project and execution of the project experimental tests. Dr. Mark Iadiacola of the National Institute of Standards and Technology is thanked for his substantive input and assistance with the experimental data. The opinions, findings and conclusions expressed in this paper are those of the authors and do not necessarily reflect the views of the above individuals, organizations, and program sponsors.

References

FHWA (2012). "Guidelines for the Load and Resistance Factor Design and Rating of Riveted and Bolted Gusset-Plate Connections for Steel Bridges", Project No. 12-84, Draft Final Report, April.

FHWA (2009). "Load Rating Guidance and Examples for Bolted and Riveted Gusset Plates in Truss Bridges", Publication No. FHWA-IF-09-014, US Department of Transportation, Federal Highway Administration, February, 44 pp.

FHWA (2008). "Load-carrying Capacity Considerations of Gusset Plates in Non-load-path-redundant Steel Truss Bridges", Technical Advisory 5140.29, Federal Highway Administration, Washington, DC, 2 pp.

Holt, R. and Hartmann, J. (2008). "Adequacy of the U10 and L11 Gusset Plate Designs for the Minnesota Bridge No. 9340 (I-35W Over the Mississippi River)", Interim Report, Turner-Fairbank Highway Research Center. Federal Highway Administration, January 11, 16 pp.

NTSB (2008). "Collapse of I-35W Highway Bridge, Minneapolis, Minnesota, August 1, 2007", Highway Accident Report NTSB/HAR-08/03, Washington, D.C.

Mentes, Y. (2011). "Analytical and Experimental Assessment of Steel Truss Bridge Gusset Plate Connections", Ph.D. Dissertation, School of Civil and Environmental Engineering, Georgia Institute of Technology, December 2011, 470 pp.

Simulia (2010). "Abaqus Analysis User Manual, Version 6.10", Providence, R.I.

White, D.W., Leon, R.T., Kim, Y.D., Mentes, Y., and Bhuiyan, M. T. (2013). "Finite Element Simulation and Assessment of the Strength Behavior of Riveted and Bolted Gusset-Plate Connections in Steel Truss Bridges", Report prepared for Federal Highway Administration and NCHRP Transportation Research Board of the National Academies.